CHEMPHYSCHEM

Supporting Information

Optimized NMR Experiments for the Isolation of *I*=½ Manifold Transitions in Methyl Groups of Proteins

Vitali Tugarinov,* Theodoros K. Karamanos, Alberto Ceccon, and G. Marius Clore*

Description of the evolution of magnetization during the pulse-schemes for $I = \frac{1}{2}$ manifold selection using single transition spin operators.

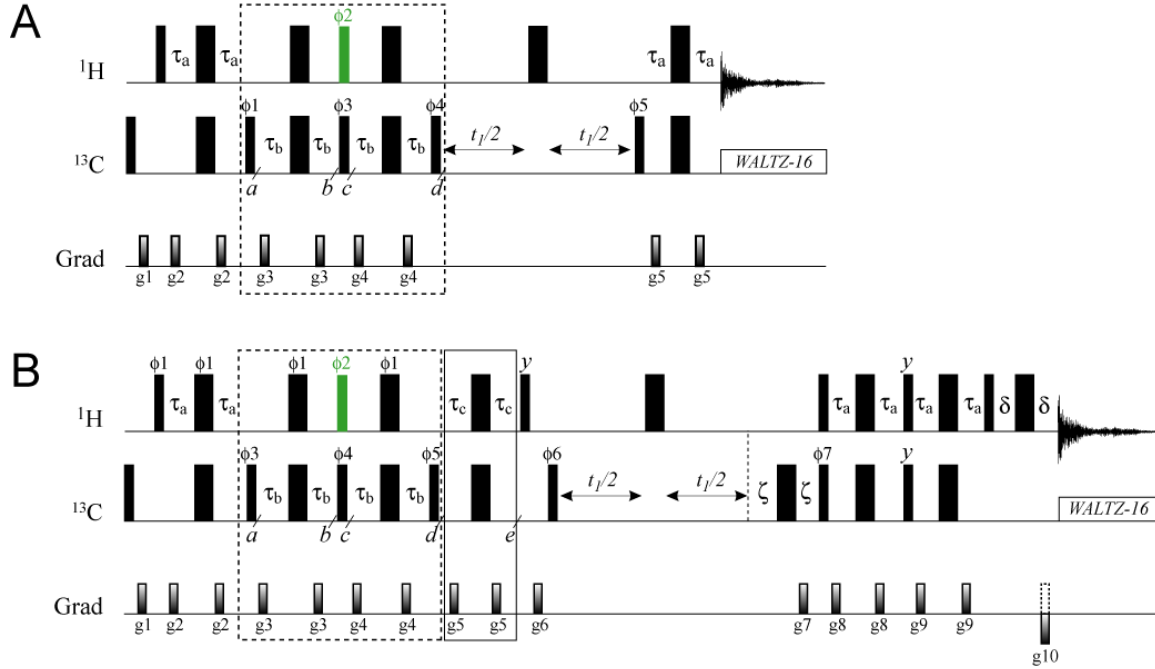**Figure S1.** Pulse sequences for separation of $I = 1/2$ manifold transitions in $^{13}CH_3$ methyl groups with (**A**) an HMQC-'read-out', and (**B**) active elimination of ^1H triple-quantum (TQ) coherences and a gradient-selected sensitivity enhanced HSQC 'read-out' scheme. All narrow and wide rectangular pulses are applied with flip angles of 90° and 180°, respectively, along the x-axis unless indicated otherwise. The ^1H pulse shown in green is applied with flip angle $\alpha = \sin^{-1}(2/3) = 41.81°$. The ^1H and ^{13}C carrier frequencies are positioned in the center of the Ileδ1-Leu-Val methyl region - 0.5 and 20 ppm, respectively, or at 1.5 and 19 ppm, respectively, for Alaβ-labeled samples. All ^1H and ^{13}C pulses are applied with the highest possible power, while ^{13}C WALTZ-16 decoupling[1] is achieved using a 2-kHz field. (**A**) Delays are: $\tau_a = 1/(4J_{HC}) = 2.0$ ms; $\tau_b = 1/(8J_{HC}) = 1.0$ ms. The durations and strengths of pulsed-field gradients in units of (ms; G/cm) are: g1 = (1; 25), g2 = (0.5; 15), g3 = (0.3; 10), g4 = (0.4; 12), g5 = (0.35; 15). The phase cycle is: $\phi1 = x,-x$; $\phi2 = 2(y),2(-y)$; $\phi3 = y,-y$; $\phi4 = 4(y),4(-y)$; $\phi5 = x$; rec. $= 4(x,-x)$. (**B**) Delays τ_a and τ_b are the same as in (A); $\tau_c = 1/(12J_{HC}) = 667$ μs; $\delta = 500$ μs; $\zeta = 400$ μs. The durations and strengths of pulsed-field gradients g1 through g4 are the same as in (A). Other gradients in units of (ms; G/cm) are: g5 = (0.5; 20), g6 = (1.2; 25), g7 = (0.2; 35), g8 = (0.3; 12), g9 = (0.4; 15), g10 = (0.053; 35). The phase cycle is $\phi1 = x$; $\phi2 = 2(y),2(-y)$; $\phi3 = 2(x),2(-x)$; $\phi4 = y,-y$; $\phi5 = 4(x),4(-x)$; $\phi6 = x,-x$; $\phi7 = x$; receiver $= x,-x,-x,x,-x,x,x,-x$. When the element enclosed in solid rectangle is omitted, the phase cycle is: $\phi1 = (0°,60°)$; $\phi2 = (90°,150°,270°,330°)$ and the rest of the phases are as above. Quadrature detection in t_1 is achieved via the States[2] incrementation of $\phi5$ in (A) and the Rance-Kay gradient selection scheme,[3,4] whereby $\phi7$ is inverted together with the gradient g10 for each point in t_1, in (B).

The pulse schemes start with the preparation of $^{13}CH_3$ methyl magnetization in a state where only the central (slowly relaxing) coherences of all manifolds (shown with red arrows in Fig. 1, main text) are present using the pulse elements described previously.[5] At time-point a in the schemes, the coherence of interest is $\rho_a = 2I_XC_Y$, where A_Q is the $Q \in \{X, Y, Z\}$ component of A spin operator, and $2I_XC_Y$ is given by,

1

$$2I_X C_Y = 2I_X^{3/2,F} C_Y + 2I_X^{3/2,S} C_Y + 2I_X^{1/2,A} C_Y + 2I_X^{1/2,B} C_Y \tag{S1}$$

where the superscripts '3/2' and '1/2' indicate that the coherence derives from the $I = 3/2$ or 1/2 manifold, the superscripts 'F' or 'S' indicate the fast and slowly relaxing coherences, respectively, from the $I = 3/2$ manifold, and the superscripts 'A' and 'B' distinguish between the two $I = 1/2$ manifolds. Written in terms of individual transitions, with the eigenfunctions $|j\rangle$ defined as in Fig. 1 of the main text, the operators I_Q are given by,

$$
\begin{aligned}
I_X^{3/2,F} &= \frac{\sqrt{3}}{2}(|1\rangle\langle 2| + |2\rangle\langle 1| + |3\rangle\langle 4| + |4\rangle\langle 3|) \\
I_X^{3/2,S} &= 1(|2\rangle\langle 3| + |3\rangle\langle 2|) \\
I_X^{1/2,A} &= \frac{1}{2}(|5\rangle\langle 6| + |6\rangle\langle 5|) \\
I_X^{1/2,B} &= \frac{1}{2}(|7\rangle\langle 8| + |8\rangle\langle 7|)
\end{aligned}
\tag{S2}
$$

Immediately after the $2\tau_b$ period at time-point b,

$$\rho_b = -2I_{X,A}^{3/2,F} C_X + 2I_X^{3/2,S} C_Y + 2I_X^{1/2,A} C_Y + 2I_X^{1/2,B} C_Y, \tag{S3}$$

where

$$I_{X,A}^{3/2,F} = \frac{\sqrt{3}}{2}(|1\rangle\langle 2| + |2\rangle\langle 1| - |3\rangle\langle 4| - |4\rangle\langle 3|). \tag{S4}$$

The phase of the subsequent ^{13}C 90° pulse is cycled along $\pm y$ while retaining the phase of the receiver, so that the $-2I_{X,A}^{3/2,F} C_X$ term is eliminated, and the state of the spin-system is thus prepared for subsequent manipulation.

Simultaneously with the ^{13}C 90°$_{\pm y}$ pulse, a ^{1}H pulse of angle $\alpha = \sin^{-1}(2/3)$ is applied (shown in green in Fig. S1) that 'nulls' the slow-relaxing ^{1}H transitions of the $I = 3/2$ manifold, 're-creates' a portion of fast-relaxing ^{1}H transitions, and produces a mixture of ^{1}H coherences, double quantum, 'DQ', triple-quantum, 'TQ', and zero-quantum, 'ZQ' (diagonal elements of the density matrix). Below, we provide a

formal derivation of the state of the density matrix (^{1}H magnetization only) at time-point c of the pulse schemes in Fig. S1 (ρ_c) for an arbitrary flip-angle α of the ^{1}H $90_{\phi2}$ pulse.

The density matrix describing the state of the ^{1}H magnetization in a (^{13}C)H$_3$ spin-system and ^{1}H RF pulse operators can be separated onto the parts corresponding to the $I = 3/2$ and $I = 1/2$ manifolds, as they evolve independently of each other under the effect of RF field (they can be coupled through relaxation processes only). The operators of a ^{1}H pulse of phase y are defined as,

$$
I_y^{3/2} = i \begin{bmatrix} 0 & -\sqrt{3}/2 & 0 & 0 \\ \sqrt{3}/2 & 0 & -1 & 0 \\ 0 & 1 & 0 & -\sqrt{3}/2 \\ 0 & 0 & \sqrt{3}/2 & 0 \end{bmatrix} \tag{S5.1}
$$

for the $I = 3/2$ manifold, and

$$
I_y^{1/2} = i \begin{bmatrix} 0 & -1/2 & 0 & 0 \\ 1/2 & 0 & 0 & 0 \\ 0 & 0 & 0 & -1/2 \\ 0 & 0 & 1/2 & 0 \end{bmatrix} \tag{S5.2}
$$

for the two $I = \frac{1}{2}$ manifolds, operating on the column-vectors of eigenfunctions $[|1>, |2>, |3>, |4>]^T$ and $[|5>, |6>, |7>, |8>]^T$, respectively, where the eigenfunctions are defined in the energy level diagram of Fig. 1 (main text) and superscript 'T' denotes transposition.

The evolution of the 4x4 density matrices $\rho^{1/2}$ and $\rho^{3/2}$ under the application of a RF pulse of flip-angle α, is described by the relationship,

$$
\rho(\alpha) = e^{-i\alpha I_y} \rho e^{i\alpha I_y} \tag{S6}
$$

and can be calculated using the expansion of the matrix exponential,

$$
e^{i\alpha I_y} = \sum_{k=0}^{3} \beta_k I_y^k = \beta_0 E + \beta_1 I_y + \beta_2 I_y^2 + \beta_3 I_y^3 \tag{S7}
$$

where E is a 4x4 identity matrix. The coefficients β can be determined from the system of equations constructed via application of the Cayley-Hamilton theorem using the relationship,

$$e^{i\alpha\lambda_i} = \sum_{k=0}^{3} \beta_k \lambda_i^k \tag{S8}$$

where λ_i is the ith eigenvalue of I_y; the number of equations $i = 1, \ldots n$, where n is the number of unique eigenvalues of I_y. There are four unique eigenvalues of $I_y^{3/2}$: {-3/2; -1/2, 1/2, 3/2}, and,

$$e^{i\alpha I_y^{3/2}} = \frac{1}{8}[9\cos(\alpha/2) - \cos(3\alpha/2)]E + \frac{i}{4}[9\sin(\alpha/2) - \frac{1}{3}\sin(3\alpha/2)]I_y^{3/2}$$
$$+ \frac{1}{2}[\cos(3\alpha/2) - \cos(\alpha/2)]\{I_y^{3/2}\}^2 + \frac{i}{3}[\sin(3\alpha/2) - 3\sin(\alpha/2)]\{I_y^{3/2}\}^3 \tag{S9}$$

while $I_y^{1/2}$ has only two unique eigenvalues: {-1/2; 1/2}, and therefore, $\beta_0 = \cos(\alpha/2)$, $\beta_1 = 2i\sin(\alpha/2)$, $\beta_2 = \beta_3 = 0$, and

$$e^{i\alpha I_y^{1/2}} = \cos(\alpha/2)E + 2i\sin(\alpha/2)I_y^{1/2} \tag{S10}$$

The forms of the density matrices describing the states of the ^1H magnetization at time-point b of the schemes in Fig. S1 are given by,

$$\rho_b^{3/2} = \begin{bmatrix} 0 & 0 & 0 & 0 \\ 0 & 0 & 1 & 0 \\ 0 & 1 & 0 & 0 \\ 0 & 0 & 0 & 0 \end{bmatrix} \tag{S11.1}$$

for the $I = 3/2$ manifold, and

4

$$\rho_b^{1/2} = \frac{1}{2}\begin{bmatrix} 0 & 1 & 0 & 0 \\ 1 & 0 & 0 & 0 \\ 0 & 0 & 0 & 1 \\ 0 & 0 & 1 & 0 \end{bmatrix} \tag{S11.2}$$

for the two $I = \frac{1}{2}$ manifolds. Using expansions of Eqs. (S9) and (S10), the form of the density matrix of each manifold at time-point c (after the $90°$ ^{13}C pulse and the $^1H_{\phi 2}$ pulse of angle α) can be calculated via Eq. (S6). After somewhat lengthy but straightforward calculations, we obtain,

$$\rho_c^{3/2}(\alpha) = \frac{1}{4}\begin{bmatrix} -3\sin^3\alpha & -3\sqrt{3}\cos\alpha(\cos^2\alpha-1) & \sqrt{3}\sin\alpha(3\sin^2\alpha-2) & 3\cos\alpha(\cos^2\alpha-1) \\ -3\sqrt{3}\cos\alpha(\cos^2\alpha-1) & 9\sin^3\alpha-8\sin\alpha & \cos\alpha\ (9\cos^2\alpha-5) & -\sqrt{3}\sin\alpha(3\sin^2\alpha-2) \\ \sqrt{3}\sin\alpha(3\sin^2\alpha-2) & \cos\alpha\ (9\cos^2\alpha-5) & 8\sin\alpha-9\sin^3\alpha & -3\sqrt{3}\cos\alpha(\cos^2\alpha-1) \\ 3\cos\alpha(\cos^2\alpha-1) & -\sqrt{3}\sin\alpha(3\sin^2\alpha-2) & -3\sqrt{3}\cos\alpha(\cos^2\alpha-1) & 3\sin^3\alpha \end{bmatrix} \tag{S12}$$

The corresponding density matrix of the $I = \frac{1}{2}$ manifold is given by,

$$\rho_c^{1/2}(\alpha) = \frac{1}{2}\begin{bmatrix} -\sin\alpha & \cos\alpha & 0 & 0 \\ \cos\alpha & \sin\alpha & 0 & 0 \\ 0 & 0 & -\sin\alpha & \cos\alpha \\ 0 & 0 & \cos\alpha & \sin\alpha \end{bmatrix} \tag{S13}$$

Thus, for an arbitrary angle α, the density matrix ρ_c at time-point c of the scheme in Fig. S1, can be written as,

$$\rho_c = \{2\cos\alpha(9\cos^2\alpha - 5)\}I_X^{3/2,S}C_Y + \{2\cos\alpha\}I_X^{1/2,A}C_Y + \{2\cos\alpha\}I_X^{1/2,B}C_Y + 2aI_X^{3/2,F}C_Y$$
$$+2cI_{TQ}^{3/2}C_Y + 2bI_{DQ}^{3/2}C_Y + 2dI_{ZQ}^{3/2,out}C_Y + 2eI_{ZQ}^{3/2,in}C_Y + \{2\sin\alpha\}I_{ZQ}^{1/2,A}C_Y + \{2\sin\alpha\}I_{ZQ}^{1/2,B}C_Y \tag{S14}$$

where $I_X^{3/2,F}$, $I_X^{3/2,S}$, $I_X^{1/2,A}$ and $I_X^{1/2,B}$ are defined in Eq. (S2), $a = -\frac{3}{2}\cos\alpha(\cos^2\alpha-1)$, and

$$I_{DQ}^{3/2} = (|1><3|+|3><1|-|2><4|-|4><2|); \quad b = \frac{\sqrt{3}}{4}\sin\alpha(3\sin^2\alpha - 2);$$

$$I_{TQ}^{3/2} = (|1><4|+|4><1|); \quad c = \frac{3}{4}\cos\alpha(\cos^2\alpha - 1);$$

$$I_{ZQ}^{3/2,out} = (|1><1|-|4><4|); \quad d = -\frac{3}{4}\sin^3\alpha; \tag{S15}$$

$$I_{ZQ}^{3/2,in} = (|2><2|-|3><3|); \quad e = -\frac{1}{4}(8\sin\alpha - 9\sin^3\alpha);$$

$$I_{ZQ}^{1/2,A} = \frac{1}{2}(|6><6|-|5><5|); \quad I_{ZQ}^{1/2,B} = \frac{1}{2}(|8><8|-|7><7|).$$

where the subscripts ('*DQ*'; '*ZQ*'; '*TQ*') denote the order of ^{1}H coherences, and the superscripts '*out*' and '*in*' distinguish the 'outer' and 'inner' polarizations within the $I = 3/2$ manifold. When the angle of the pulse α is adjusted to $\sin^{-1}(2/3) = 41.81°$, the inner transitions of the $I = 3/2$ manifold, $I_X^{3/2,S}$, vanish: $(9\cos^2\alpha - 5) = 0$ in the first term of Eq. (S14) (the elements [2,3] and [3,2] of the matrix in Eq. (S12) shown in bold), while the remaining portion of the $I = 1/2$ manifold magnetization is equal to $\cos(\alpha) = 0.7454$ (~3/4 of the starting value). The cycling of the phase of the ^{1}H$_{\phi 2}$ α pulse, ±*y*, with the concomitant retention of the receiver phase eliminates all the ^{1}H coherences of even order (ZQ and DQ; the last five terms in Eq. (S14)), as the inversion of the phase of this pulse changes the signs of only these latter terms while preserving those of the ^{1}H coherences of odd order (single-quantum, SQ, and TQ; the first five terms in Eq. (S14)). Further, re-created fast-relaxing coherences corresponding to the outer transitions of the $I = 3/2$ manifold, $I_X^{3/2,F}$, can be eliminated by the second application of the ^{1}H-^{13}C multiple-quantum *J*-filter of duration $2\tau_b$ and the associated phase-cycling of the subsequent ^{13}C 90° pulse ($\phi 4$ in Fig. S1A), ±*y*, so that at time-point *d* of the scheme in Fig. S1A, the state of the density matrix can, to within a multiplication factor, be described by,

$$\rho_d^{S1A} = 2(\sqrt{5}/3)I_X^{1/2,A}C_Y + 2(\sqrt{5}/3)I_X^{1/2,B}C_Y - 2(\sqrt{5}/9)I_{TQ}^{3/2}C_Y \tag{S16}$$

If the order of ^{1}H coherences is not 'perturbed' in the rest of the experiment, *i.e.* a 'read-out' scheme is used that does not involve ^{1}H pulses other than 180° as is the case, for example, of HMQC-type experiments,[6,7] the selection of the $I = 1/2$ manifold transitions occurs 'naturally', as the third term in Eq. (S16) containing ^{1}H TQ coherences will not lead to observable magnetization at the end of the experiment (during acquisition). Such a pulse scheme is shown in Fig. S1A.

A pulse scheme that uses a sensitivity-enhanced HSQC 'read-out' is shown in Fig. S1B. Here, the terms containing the outer transitions of the $I = 3/2$ manifold, $I_X^{3/2,F}$, are eliminated by cycling the phase of the ^{13}C $90_{\phi5}$ pulse, $\pm x$, with concomitant inversion of the receiver phase, so that at time-point d in the experiment of Fig. S1B, the state of the density matrix is given by,

$$\rho_d^{\text{S1B}} = 2(\sqrt{5}/3)I_X^{1/2,A}C_Z + 2(\sqrt{5}/3)I_X^{1/2,B}C_Z - 2(\sqrt{5}/9)I_{TQ}^{3/2}C_Z \tag{S17}$$

The third term in Eq. (S17) containing ^{1}H TQ coherences is eliminated by the application of a 'filter' of duration $2\tau_c = 1/(6J_{\text{CH}})$. As ^{1}H TQ coherences evolve due to scalar coupling to the ^{13}C spin three times faster than SQ ^{1}H magnetization (the first two terms in Eq. (S17)), after the delay $2\tau_c$ ^{1}H TQ coherences evolve to become in-phase with respect to the ^{13}C spin, $\sim (\sqrt{5}/9)\,I_{TQ}^{3/2}$, and are eliminated by the gradient g6 and the phase-cycling of the subsequent ^{13}C $90°_{\phi6}$ pulse. The remaining part of the ^{1}H SQ magnetization deriving from the $I = 1/2$ manifold after the $2\tau_c$ period is equal to $\cos(\pi/6) = \sqrt{3}/2$, corresponding to a loss of less than 14 %. An alternative strategy for elimination of the ^{1}H TQ-containing terms is a two-step phase cycling of all ^{1}H pulses up to the first ^{1}H$_y$ pulse (phases $\phi1$ and $\phi2$ in Fig. S1B) with an increment of 60° (0°; 60°) while the receiver phase is retained. The remaining fraction of the ^{1}H SQ $I = 1/2$ magnetization in this case is equal to 3/4, a loss of 25 %. Unless significant relaxation losses are expected during the $2\tau_c$ period (as would be the case for very large proteins), we prefer the 'filtering' approach above as it is less costly in sensitivity. Irrespective of the method of choice for selection against the ^{1}H TQ-containing terms in Eq. (S17), the magnetization after time-point e in Fig. S1B can then be manipulated as an AX (^{1}H-^{13}C) spin-system.

Pulse scheme for a single-quantum methyl-^{1}H CPMG relaxation dispersion experiment with $I = 1/2$ manifold selection.

Figure S2. Pulse scheme for a single-quantum ^{1}H CPMG relaxation dispersion experiment with $I = \frac{1}{2}$ manifold selection. All narrow and wide rectangular pulses are applied with flip angles of 90 and 180°, respectively, along the x-axis unless indicated otherwise. The ^{1}H pulse shown in green is applied with a flip angle $\alpha = \sin^{-1}(2/3) = 41.81°$. The ^{1}H and ^{13}C carrier frequencies are positioned in the center of the Ileδ1-Leu-Val methyl region - 0.5 and 20 ppm, respectively. All ^{1}H and ^{13}C pulses are applied with the highest possible power, except for the ^{1}H pulses during the CPMG period shown with open rectangles that are applied with a 25 kHz radiofrequency (RF) field and implemented as composite $90°_{\theta-\pi/2}\text{-}240°_{\theta}\text{-}90°_{\theta-\pi/2}$ pulses.[8] A 2-kHz RF field was used for ^{13}C WALTZ-16[1] decoupling. Delays are: $\tau_a = 1/(4J_{HC}) = 2.0$ ms; $\tau_b = 1/(8J_{HC}) = 1.0$ ms; $\tau_c = 1/(12J_{HC}) = 667$ µs; $\delta = 500$ µs; $\zeta = 400$ µs. The delay τ_{cp} is half that of the interval between CPMG pulses. N is the total number of CPMG cycles (can be even or odd). The durations and strengths of pulsed-field gradients in units of (ms; G/cm) are: g1 = (1; 25), g2 = (0.5; 15), g3 = (0.3; 10), g4 = (0.4; 12), g5 = (0.5; 20), g6 = (1.2; 25), g7 = (0.2; 35), g8 = (0.3; 12), g9 = (0.4; 15), g10 = (0.053; 35). The phase cycle is $\phi1 = x$; $\phi2 = 2(y),2(-y)$; $\phi3 = 2(x),2(-x)$; $\phi4 = y,-y$; $\phi5 = 4(x),4(-x)$; $\phi6 = 8(-x),8(x)$; $\phi7 = x,-x$; $\phi8 = x$; the phases ψ1/ψ3 follow the XY-4 scheme:[9] ψ1 is incremented with a cycle (x,y,x,y) for each successive pulse in the CPMG train, and ψ3 decremented in the same manner but inverted; $\psi2 = y,-y$; rec. $= x,-x,x, -x,x,x,-x, -x,x,x,-x, x,-x,-x,x$. When the element enclosed by the solid rectangle is omitted, the phase cycle is: $\phi1 = (0°,60°)$; $\phi2 = (90°,150°,270°,330°)$; $\phi3 = 2(x),2(-x)$; $\phi4 = y,-y$; $\phi5 = 4(x),4(-x)$; $\phi7 = x,-x$; $\phi8 = x$; receiver = $x,-x,-x,x, -x,x,x,-x$. and the phases ψ are as above. Quadrature detection in t_1 is achieved using the Rance-Kay gradient selection scheme,[3,4] whereby $\phi8$ is inverted together with the gradient g10 for each complex point in t_1.

Fig. S3 shows comparisons of selected SQ ^{1}H CPMG relaxation dispersion profiles obtained for {[13]CH$_3$}-labeled ΔST-DNAJB6b using the $I = 1/2$ manifold selection scheme in Fig. S2 and the compensated methyl-TROSY-based CPMG experiment.[10] At the protein concentration used for CPMG experiments (200 µM), ΔST-DNAJB6b is known to interconvert at a rate of ~1500 s^{-1} between the free, major state A and a minor state B populated at ~2 % and corresponding to a high-molecular-weight assembly composed of ~35 units of ΔST-DNAJB6b.[11] For methyl sites not participating in exchange (Fig. S3A), large differences in the effective rates $R_{2,\text{eff}}$ can be noted between the two experiments, as the fast-relaxing ^{1}H coherences are not actively eliminated in the scheme of Yuwen et al.[10] and therefore contribute to the effective rate in the moderately-sized ΔST-DNAJB6b. For methyl sites showing significant relaxation dispersion (Fig. S3B), the contribution of exchange to the effective rate (R_{ex}) is considerably higher in the

I = 1/2 manifold selected CPMG experiment because both states A and B have lower effective transverse spin relaxation rates, $R_{2,A}$ and $R_{2,B}$, the latter affecting the size of the dispersion (R_{ex}) to a significant extent. This effect should be distinguished from the inherent (slight) reduction in R_{ex} in the compensated methyl-TROSY-based CPMG experiment discussed in Yuwen *et al.*[10] (see SI, Fig. S7, of ref. [10]).
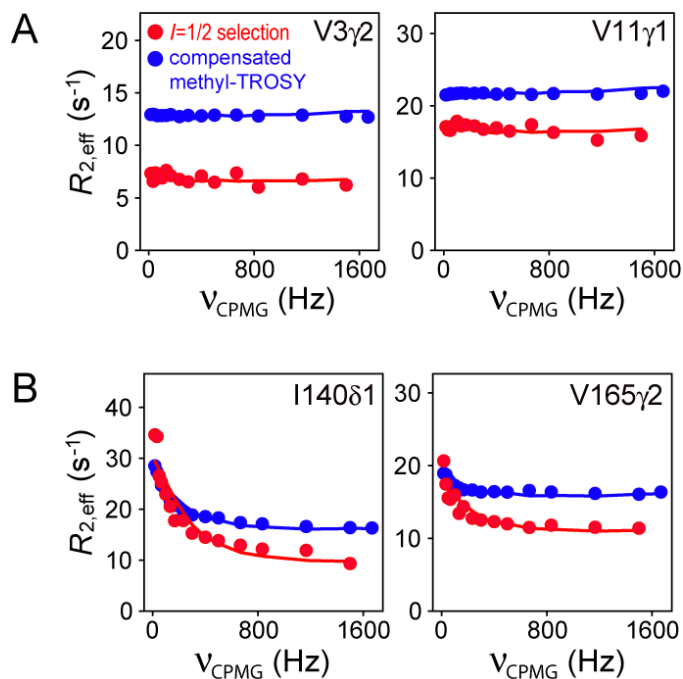

Figure S3. Examples of SQ ^{1}H CPMG relaxation dispersion profiles obtained for selected residues of {U-[^{15}N,^{2}H]; Ileδ1-[^{13}CH$_3$]; Leu,Val-[^{13}CH$_3$,^{12}CD$_3$]}-labeled ΔST-DNAJB6b (500 MHz; 25 °C) with the I = 1/2 manifold selection scheme of Fig. S2 (red), and the compensated methyl-TROSY-based CPMG experiment of Yuwen *et al.*[10] (blue). A constant-time period T_{relax} of 60 ms was used in both experiments. Panel **A** shows examples of residues not participating in the exchange process (flat profiles are expected), while the residues that inter-convert with a minor, high-molecular-weight state B are shown in panel **B**.

Estimation of the robustness of the experiment for RDC measurements (Fig. 4A, main text) with respect to deviations of (J_{CH} + D_{CH}) couplings from their nominal value of 125 Hz in the absence of alignment.

Deviations of the effective coupling constants (J_{CH} + D_{CH}) in RDC measurements from the nominal value of $^1J_{CH}$ = 125 Hz for which all the delays are tuned in the experiments of Fig. 2 and Fig. 4A (main text), will inevitably compromise to some extent the selection of the I = 1/2 manifold coherences. In particular, for J_{CH} + D_{CH} ≠ 125 Hz, some SQ ^{13}C coherences belonging to the I = 3/2 manifold (corresponding to both outer, fast-relaxing and inner, slow-relaxing ^{13}C transitions) will be present during the constant-time period T (Fig. 4A, main text). While the inner, slow-relaxing transitions of the I = 3/2 manifold cannot by themselves compromise the measurements of the (J_{CH} + D_{CH}) couplings as they evolve in the same manner as the ^{13}C coherences of the I = 1/2 manifold, $\cos(\pi[J_{CH} + D_{CH}]t_2)$, their outer, fast-relaxing counterparts that evolve as $\cos(3\pi[J_{CH} + D_{CH}]t_2)$, can potentially be detrimental for the accurate derivation of (J_{CH} + D_{CH}) couplings. To estimate the contributions of these latter coherences, we calculated their fraction F of the total observable signal at the end of the experiment in Fig. 4A (main text) using ^{1}H and ^{13}C relaxation rates predicted theoretically for ΔST-DNAJB6b in D_2O solvent (rotational correlation time τ_C ~ 14 ns) (Fig. S4). Since relaxation in these calculations was taken into account only during the constant-time period T and direct acquisition period in the scheme of Fig. 4A (and neglected during all periods $2\tau_a$, $2\tau_b$ and $2\tau_c$ of the scheme), the values of F in Fig. S4 are likely to be overestimates by absolute magnitude. Note that while scalar (J_{CH}) couplings in Ile, Leu and Val methyls of proteins are very homogeneous (125 ± 1.5 Hz), methyl ^{1}H-^{13}C RDCs (D_{CH}) are scaled down by a factor of -1/3 by fast internal rotation of a methyl group around the three-fold symmetry axis, with experimental values of D_{CH} in ΔST-DNAJB6b never exceeding ~11 Hz by absolute magnitude. Although no detrimental effects of the 'contamination' of the signal by fast-relaxing ^{13}C coherences during time-period T on the extracted values of D_{CH} was observed in practice in ΔST-DNAJB6b, we note that if the experiment is applied to the measurements of methyl RDCs in smaller proteins and/or with stronger alignment, the use of longer constant-time periods T is recommended to reduce the fractions F to undetectable quantities.
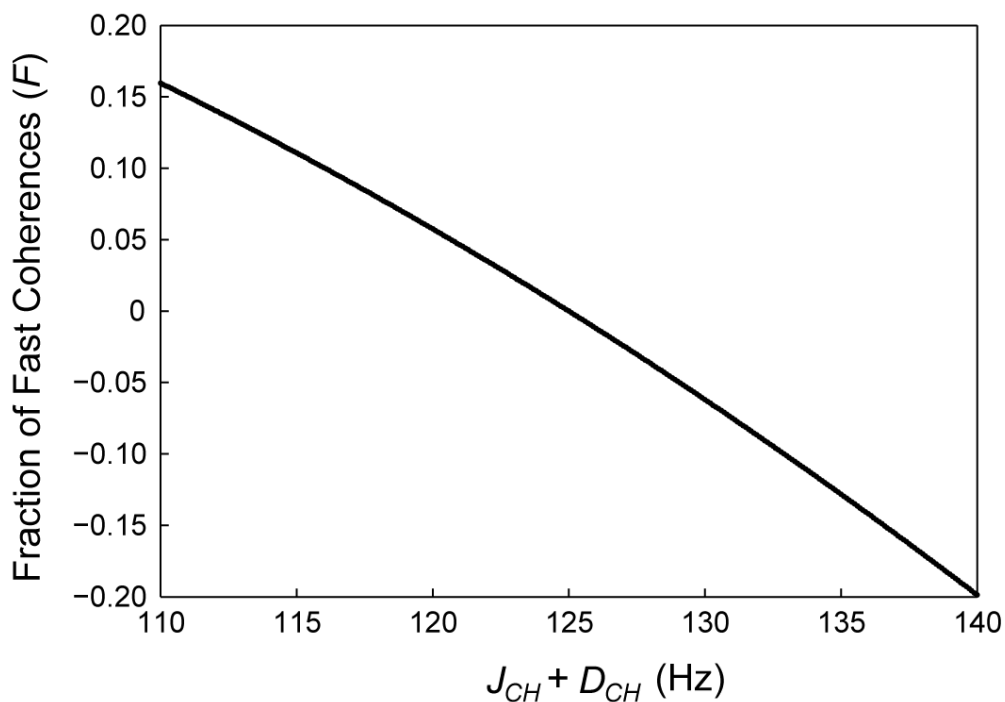
Figure S4. A plot of the fraction (F) of fast-relaxing coherences during the constant-time period T that contribute to the total observable signal at the end of the experiment in Fig. 4A, main text (y-axis) as a function of the value of the effective coupling, $J_{CH} + D_{CH}$, (x-axis). The calculations were performed by taking the trace of the product of the full (16x16) density matrix of a $^{13}CH_3$ group at the end of the experiment of Fig. 4A (main text) and the observation operator H_-, $tr(\rho H_-)$, with (1) only the outer, fast-relaxing SQ ^{13}C coherences, or (2) all SQ ^{13}C coherences included during the constant-time period T. The following acquisition parameters were used in the calculations: $T = 28$ ms, (direct) acquisition time acq = 64 ms, and all the delay durations as specified in Fig. S1 for a nominal value of $^1J_{CH} = 125$ Hz. The following transverse spin relaxation rates were used: fast- and slow-relaxing ^{13}C coherences, 37 and 7 s^{-1}, respectively, during the period T, and fast- and slow-relaxing ^1H coherences, 71 and 9.5 s^{-1}, respectively, during acquisition. These spin relaxation rates were calculated using the relationships that can be found in ref. [12], where standard methyl geometry and ^1H-^{13}C inter-nuclear distance $r_{CH} = 1.135$ Å were used. Effective distances $r_{HH,ext} = 3.5$ Å and $r_{HD,ext} = 1.8$ Å to single external ^1H and ^2H spins were used. The global rotational correlation time τ_C was set to 14 ns, while the order parameters squared for intra-methyl interactions and interactions with external ^1H and ^2H spins were set to 0.7 and 1.0, respectively.

Materials and Methods

NMR Sample Preparation. The samples of {U-[^{15}N,^{2}H]; Ileδ1-[^{13}CH$_3$]; Leu,Val-[^{13}CH$_3$,^{12}CD$_3$]}-labeled and {U-[^{15}N,^{2}H]; Ileδ1-[^{13}CHD$_2$]; Leu,Val-[^{13}CHD$_2$,^{12}CD$_3$]}-labeled human ubiquitin (8.5 kDa) were prepared as described in detail previously[13] using U-[^{2}H]-D-glucose as the main carbon source and the appropriate α-keto-acid precursors for selective methyl labeling. Sample conditions were: 1.3 mM protein, 99.9% D$_2$O, 25 mM sodium phosphate, pH 6.7 (uncorrected). The samples of {U-[^{15}N,^{2}H]; Alaβ-[^{13}CH$_3$]}-labeled and {U-[^{15}N,^{2}H]; Alaβ-[^{13}CHD$_2$]}-labeled MSG (82 kDa) were prepared as described previously.[14] The concentration of MSG was 0.65 mM in a buffer comprising 99.9% D$_2$O, 25 mM sodium phosphate (pH 7.0; uncorrected), 5 mM MgCl$_2$ and 0.05% NaN$_3$. The sample of {U-[^{15}N,^{2}H]; Ileδ1-[^{13}CH$_3$]; Leu,Val-[^{13}CH$_3$,^{12}CD$_3$]}-labeled ΔST-DNAJB6b was prepared as described elsewhere,[11] but without removal of the Histidine tag. Sample conditions were: 200 μM ΔST-DNAJB6b, 99.9% D$_2$O, 20 mM sodium phosphate, pH 7.0 (uncorrected) and 50 mM NaCl.

It is important to emphasize the importance of high levels of deuteration to the methodology presented in this work. The use of perdeuterated, selectively methyl-labeled samples[15,16] eliminates ^{1}H-^{1}H scalar couplings that otherwise would adversely affect the efficiency of $I = ½$ manifold selection.

NMR Spectroscopy. NMR measurements on human ubiquitin (at 5 and 25 °C) and MSG (37 °C) were performed at 500 MHz (^{1}H frequency) on a Bruker Avance spectrometer equipped with a room-temperature triple-resonance *x,y,z*-gradient probe, while the experiments on ΔST-DNAJB6b were carried out at 600 MHz, 25 °C, using a Bruker Avance HD 600 MHz spectrometer with a triple-resonance *z*-gradient cryo-probe. NMR experiments acquired with the pulse schemes shown in Fig. 2, main text, and Fig. S1, on ubiquitin samples were typically obtained with 8 scans/FID, (512; 64) complex points in (t_2; t_1), and an inter-scan recovery delay of 1 s, resulting in net acquisition time of ~20 min. The same spectra on Alaβ-labeled MSG samples used 16 scans/FID, (512; 64) complex points in (t_2; t_1), and an inter-scan recovery delay of 1 s, resulting in net acquisition time of ~40 min. All NMR spectra were processed and analyzed using the NMRPipe/NMRDraw suite of programs and associated software.[17]

The measurements of methyl ^{1}H-^{13}C RDCs on the {U-[^{15}N,^{2}H]; Ileδ1-[^{13}CH$_3$]; Leu,Val-[^{13}CH$_3$,^{12}CD$_3$]}-labeled sample of ΔST-DNAJB6b were performed using the scheme of Fig. 4A (main text) or a simplified version of the experiment of Ottiger *et al.*[18] with 19 evolution delays t_2 ranging from 0 to 19 ms. A constant-time period $T = 28$ ms was employed along with 32 scans/FID, (512; 128) complex points in (t_2; t_1), and an inter-scan recovery delay of 1 s, resulting in total acquisition time of ~2.5 hrs per 2D spectrum.

CPMG relaxation dispersion experiments on the {U-[^{15}N,^{2}H]; Ileδ1-[^{13}CH$_3$]; Leu,Val-[^{13}CH$_3$,^{12}CD$_3$]}-labeled sample of ΔST-DNAJB6b were performed with the following set of CPMG frequencies (ν_{CPMG}) in Hz: 17, 33, 50, 67, 100, 133, 167, 233, 300, 400, 500, 667, 833, 1167, 1500 for the I = 1/2 manifold selected experiment (Fig. S2), and 17, 33, 50, 67, 100, 133, 167, 233, 300, 400, 500, 667, 833, 1167, 1500, 1667 for the compensated methyl-TROSY based CPMG experiment of Yuwen *et al.*[10] A constant-time relaxation period of 60 ms was used in both experiments. The two CPMG experiments were collected with 64 and 16 scans/FID, (512; 128) complex points in (t_2; t_1), and an inter-scan recovery delay of 2 s, resulting in acquisition times of ~10 hrs and 2.5 hrs per 2D spectrum, for the I = 1/2 manifold selected and the compensated methyl-TROSY CPMG, respectively.

Supplementary References

[1]   A.J. Shaka, T. Keeler, T. Frenkiel, R. Freeman, *J. Magn. Reson.* **1983**, *52*, 335-338.

[2]   D.J. States, R. Haberkorn, D.J. Ruben, *J. Magn. Reson.* **1982**, *48*, 286.

[3]   J. Schleucher, M. Sattler, C. Griesinger, *Angew. Chem. Int. Ed. Engl.* **1993**, *32*, 1489-1491.

[4]   L.E. Kay, P. Keifer, T. Saarinen, *J. Am. Chem. Soc.* **1992**, *114*, 10663-10665.

[5]   V. Tugarinov, L.E. Kay, *J. Am. Chem. Soc.* **2007**, *129*, 9514-9521.

[6]   A. Bax, R.H. Griffey, B.L. Hawkings, *J. Magn. Reson.* **1983**, *55*, 301-315.

[7]   L. Mueller, *J. Am. Chem. Soc.* **1979**, *101*, 4481-4484.

[8]   M.H. Levitt, *J. Magn. Reson.* **1982**, *50*, 95-110.

[9]   T. Gullion, D.B. Baker, M.S. Conradi, *J. Magn. Reson.* **1990**, *89*, 479-484.

[10]   T. Yuwen, R. Huang, P. Vallurupalli, L.E. Kay, *Angew. Chem. Int. Ed. Engl.* **2019**, *58*, 6250-6254.

[11]   T.K. Karamanos, V. Tugarinov, G.M. Clore, *Proc. Natl. Acad. Sci. USA* **2019**, *116,* 21529-21538.

[12]   V. Tugarinov, L.E. Kay, *J. Phys. Chem. B* **2013**, *117*, 3571-3577.

[13]   A. Ceccon, V. Tugarinov, A. Bax, G.M. Clore, *J. Am. Chem. Soc.* **2016**, *138*, 5789-5792.

[14]   V. Tugarinov, R. Muhandiram, A. Ayed, L.E. Kay, *J. Am. Chem. Soc* **2002**, *124*, 10025-10035.

[15]   V. Tugarinov, L.E. Kay, *J. Biomol. NMR* **2004**, *28*, 165-172.

[16]   V. Tugarinov, V. Kanelis, L.E. Kay, *Nat. Protoc.* **2006**, *1*, 749-754.

[17]   F. Delaglio, S. Grzesiek, G.W. Vuister, G. Zhu, J. Pfeifer, A. Bax, *J. Biomol. NMR* **1995**, *6*, 277-293.

[18]   M. Ottiger, F. Delaglio, J.L. Marquardt, N. Tjandra, A. Bax, *J. Magn. Reson.* **1998**, *134*, 365-369.